ELSEVIER

Journal of Organometallic Chemistry 572 (1999) 117–123

Journal of Organometallic Chemistry

Ligand behaviour of P-functionally substituted organotin halides: synthesis, structure, and intramolecular oxidative addition of $[\{Me_2(Cl)SnCH_2CH_2PPh_2\}_2Rh(CO)Cl]$

Dirk Kruber, Kurt Merzweiler, Christoph Wagner, Horst Weichmann *

Institut für Anorganische Chemie, Martin-Luther-Universität Halle-Wittenberg, Kurt-Mothes-Straße 2, D-06120 Halle (Saale), Germany

Received 22 July 1998

Abstract

The reaction of $[Rh(CO)_2Cl]_2$ with $Me_2(Cl)SnCH_2CH_2PPh_2$ yields the square-planar rhodium(I) complex $[\{Me_2(Cl)SnCH_2CH_2PPh_2\}_2Rh(CO)Cl]$ (**1**). The crystal structure of **1** is characterized by an intramolecular Rh–Cl···Sn and an intermolecular Sn–Cl···Sn interaction. The latter gives rise to the dimerization of **1** under formation of a 16-membered macrocycle. In solution the complex is monomeric and undergoes a fast exchange between the intramolecular Rh–Cl···Sn contacts of the two ligands. By heating in toluene at 100°C, **1** transforms under elimination of methane and ethylene into the rhodium(III) complex $[\{Me(Cl)Sn\overline{CH_2CH_2PPh_2}\}_2\overline{Rh}(CO)Cl]$ (**2**). Both in solid state and in solution **2** shows a bicyclic structure with two Sn, P, and Rh containing five-membered chelate rings with a σ-Rh–Sn bond. © 1999 Elsevier Science S.A. All rights reserved.

Keywords: Rhodium stannyl complexes; Oxidative addition of Sn–C bonds; Pentacoordination; Crystal structures

1. Introduction

ω-Diphenylphosphinoalkyl triorganostannanes $R_3Sn(CH_2)_nPPh_2$ (R = Me, Ph; $n = 2, 3$) [1–3] and the distannanes $[Ph_2P(CH_2)_nMe_2Sn-]_2$ ($n = 2, 3$) [3] are suitable ligands to form phosphinoalkylstannyl chelate complexes with the structural element $[\overline{M}\leftarrow PPh_2(CH_2)_n\overline{SnR_2}$ in 'chelate assisted' oxidative additions of their Sn–C(R)– and Sn–Sn-bonds to Pd^0, Pt^0 and Fe^0 complex fragments [4–8]. The reaction of $Me_3SnCH_2CH_2PMe_2$ with $[Rh(CO)_2Cl]_2$ and $Cr(CO)_6$ yields the complexes $[\{Me_3SnCH_2CH_2PMe_2\}_2$-$Rh(CO)Cl]$ and $[(Me_3SnCH_2CH_2PMe_2)Cr(CO)_5]$. In these compounds $Me_3SnCH_2CH_2PMe_2$ acts as a monodentate ligand by P→M coordination without any interaction between the tin and transition metal [2,9].

Recently, we started investigations of the ligand behaviour of P-functionally substituted organotin halides $Me_{3-m}(X)_mSn(CH_2)_nPPh_2$ (X = Cl, $m = 1–3$; $n = 2, 3$) and related compounds in transition metal complexes [10]. In contrast to the compounds mentioned above in these ligand systems the tin atom is a centre of variable Lewis-acidity. This should have the following consequences: (i) in reactions of the ligands with transition metal complexes containing metal–halogen functions the formation of metal–halogen–tin bridges is expected. This should influence the structure and the reactivity of the resulting complexes; (ii) the formation of metallacycles by elimination of the organotin group of the ligands under formation of σ-M–C bonds (e.g. M = Pd or Pt) can occur in case of a suitable length of the $(CH_2)_n$–bridge in the ligands; (iii) finally, in reactions of $Me_{3-m}(X)_mSn(CH_2)_nPPh_2$ ($m = 2, 3$) with electron-rich low-valent metal complexes the formation of compounds with M→Sn-donor–acceptor interactions is possible which represent intermediates in oxidative additions of Sn–Hal bonds of the ligands to the metal centre [11].

* Corresponding author. Fax: +49 345 5527028; e-mail: weichmann@chemie.uni-halle.de

PII S0022-328X(98)00912-7

In this paper we report the synthesis, molecular structure, and reactivity of the complex $[\{Ph_2PCH_2CH_2Sn(Cl)Me_2\}_2Rh(CO)Cl]$.

2. Results and discussion

2.1. Synthesis

The reaction of $Me_2(Cl)SnCH_2CH_2PPh_2$ [3] with $[Rh(CO)_2Cl]_2$ in a molar ratio of 2:1 in benzene at room temperature yields the complex $[\{Me_2(Cl)SnCH_2CH_2PPh_2\}_2Rh(CO)Cl]$ (**1**) (Eq. (1)). To avoid the formation of dinuclear species solutions of the starting components in benzene are dropped simultaneously in pure benzene.

$$4Me_2(Cl)SnCH_2CH_2PPh_2 + [Rh(CO)_2Cl]_2 \xrightarrow[-2CO]{C_6H_6} 2[\{Me_2(Cl)SnCH_2\underset{1}{CH_2}PPh_2\}_2Rh(CO)Cl] \quad (1)$$

During the reaction the equivalent amount of CO is evolved. Pure **1** could be obtained by recrystallization from CH_2Cl_2/hexane. The yellow crystals melt at 124–126°C and are soluble in aromatic and chlorinated hydrocarbons. A strong absorption at 1975 cm^{-1} in the CO valence region of the IR spectrum of **1** (in CsBr) indicates a square-planar ligand arrangement at the rhodium(I) centre [2,18].

2.2. Molecular structure of $[\{Me_2(Cl)SnCH_2CH_2PPh_2\}_2Rh(CO)Cl]$ (1)

The molecular structure of **1** along with the atom-numbering scheme are shown in Fig. 1. Selected bond lengths and angles are listed in Table 1. The molecular structure of **1** shows that the two $Me_2(Cl)SnCH_2CH_2PPh_2$ ligands are both coordinated via the phosphorus atom to the rhodium atom. As a result of its Lewis acidity the tin atom of one ligand (Sn2) interacts with the chlorine atom at the rhodium centre to form a six-membered ring with an intramolecular Rh–Cl···Sn bridge. Simultaneously the same atom (Sn2) is linked with the $Me_2(Cl)Sn$-group of a neighbouring complex molecule via an intermolecular Sn(2)–Cl(2)···Sn(1′) interaction with the consequence of formation of centrosymmetric dimers. The crystallographically imposed inversion centre of the structure coincides with the midpoint of the sixteen membered macrocycle formed by the dimerization of **1**. No unusual contacts between adjacent dimeric species are observed.

The rhodium atom exhibits a square-planar coordination sphere with only slight distortion (P(1)–Rh–P(2) 179.0(1)°, Cl(1)–Rh–C(33) 176.3(2)°). The two phosphorus atoms are in the *trans* position. The Rh–Cl, Rh–P and Rh–C bond lengths are comparable with those in other complexes of the type *trans*-$[RhCl(CO)(PPh_2Alk)_2]$, e.g. *trans*-$[RhCl(CO)(PPh_2Me)_2]$ [12].

The geometry around the two tin atoms is a distorted trigonal bipyramid. In both cases the equatorial plane is occupied by three carbon atoms, belonging to the methyl groups and the P-bonded ethylene group, and one of the axial positions is occupied by the chlorine atoms Cl(2) and Cl(3), respectively. The pentacoordination is achieved in different ways: the second axial position at Sn(2) is occupied by the chlorine atom Cl(1) of the Rh–Cl function, whereas the coordination sphere around Sn(1) is completed by the chlorine atom Cl(2′) of the intermolecularly coordinated $Me_2(Cl)Sn$-$CH_2CH_2PPh_2$ ligand of a neighbouring molecule.

Comparing Sn(2) and Sn(1) the trigonal–bipyramidal skeleton of Sn(1) is distorted more towards a monocapped tetrahedron because of the stronger intramolecular Sn(2)···Cl(1) coordination than the intermolecular Sn(1)···Cl(2′) interaction. This is indicated by the smaller difference between the sums of the three equatorial and the three axial angles to the covalent bonded Cl_{ax} at Sn(1) ($\Delta\Sigma(\theta) = 52.9°$) compared with Sn(2) ($\Delta\Sigma(\theta) = 75.4°$) [13,14], the greater deviation of Sn(1)

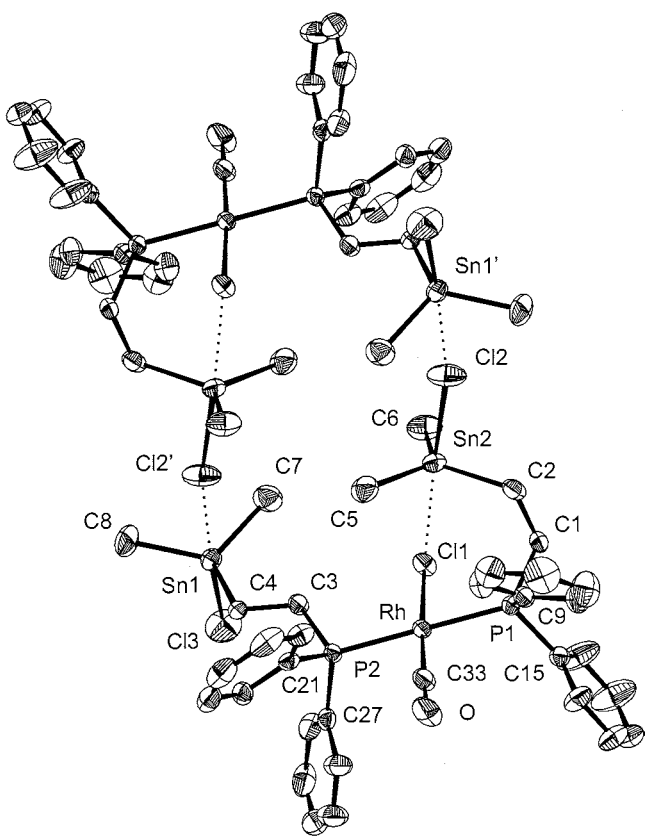

Fig. 1. Molecular structure of $[\{Me_2(Cl)SnCH_2CH_2PPh_2\}_2Rh(CO)Cl]$ (**1**) with atom-numbering. Hydrogen atoms are omitted for clarity.

Table 1
Selected bond lengths (Å), angles (°) and endocyclic torsion angles (°) for [{Me_2(Cl)Sn$CH_2CH_2PPh_2$}$_2$Rh(CO)Cl] (1)

Bond lengths (Å)			
Rh–P(1)	2.312(1)	Sn(2)–C(5)	2.118(6)
Rh–P(2)	2.336(1)	Sn(2)–C(6)	2.115(6)
Rh–Cl(1)	2.363(2)	Sn(2)–Cl(2)	2.467(2)
Rh–C(33)	1.793(5)	Sn(2)–Cl(1)	2.920(1)
Sn(1)–C(4)	2.149(4)	P(1)–C(1)	1.834(5)
Sn(1)–C(7)	2.118(6)	P(1)–C(9)	1.812(5)
Sn(1)–C(8)	2.118(6)	P(1)–C(15)	1.815(4)
Sn(1)–Cl(3)	2.405(2)	P(2)–C(3)	1.843(4)
Sn(1)–Cl(2')	3.254(2)	P(2)–C(21)	1.817(4)
Sn(2)–C(2)	2.143(5)	P(2)–C(27)	1.815(4)
Bond angles (°)			
P(1)–Rh–P(2)	179.0(1)	Cl(2)–Sn(2)–C(2)	90.7(2)
Cl(1)–Rh–C(33)	176.3(2)	Cl(2)–Sn(2)–C(5)	96.7(2)
P(1)–Rh–Cl(1)	88.8(1)	Cl(2)–Sn(2)–C(6)	95.5(2)
P(1)–Rh–C(33)	88.8(2)	Cl(2)–Sn(2)–Cl(1)	176.4(1)
P(2)–Rh–Cl(1)	92.1(1)	Rh–P(1)–C(1)	118.2(2)
P(2)–Rh–C(33)	90.4(2)	Rh–P(1)–C(9)	115.1(2)
C(4)–Sn(1)–C(7)	114.4(2)	Rh–P(1)–C(15)	111.1(1)
C(4)–Sn(1)–C(8)	120.3(3)	C(1)–P(1)–C(9)	101.8(2)
C(7)–Sn(1)–C(8)	117.1(3)	C(1)–P(1)–C(15)	102.9(2)
Cl(3)–Sn(1)–C(4)	96.9(2)	C(9)–P(1)–C(15)	106.2(2)
Cl(3)–Sn(1)–C(7)	101.5(2)	Rh–P(2)–C(3)	114.0(2)
Cl(3)–Sn(1)–C(8)	100.5(3)	Rh–P(2)–C(21)	115.0(2)
Cl(3)–Sn(1)–Cl(2')	175.0(1)	Rh–P(2)–C(27)	113.9(1)
C(2)–Sn(2)–C(5)	119.8(3)	C(3)–P(2)–C(21)	105.5(2)
C(2)–Sn(2)–C(6)	118.6(3)	C(3)–P(2)–C(27)	105.5(2)
C(5)–Sn(2)–C(6)	119.9(4)	C(21)–P(2)–C(27)	101.6(2)
Torsion angles (°)			
Rh–Cl(1)–Sn(2)–C(2)	67.5(2)	C(2)–C(1)–P(1)–Rh	68.5(5)
Cl(1)–Sn(2)–C(2)–C(1)	3.3(4)	C(1)–P(1)–Rh–Cl(1)	15.5(2)
Sn(2)–C(2)–C(1)–P(1)	−74.3(5)	P(1)–Rh–Cl(1)–Sn(2)	−65.7(1)

from the plane defined by the three equatorial carbon atoms (ΔSn(1) (plane): 0.356(4) Å; ΔSn(2)(plane): 0.160(4) Å) [14], and the shorter Sn(2)···Cl(1) distance compared with Sn(1)···Cl(2′). The last mentioned Sn···Cl distances are considerably shorter than the sum of corresponding van der Waals radii (3.85 Å [15]) and indicate substantial bonding. Finally, the small difference of 0.062 Å between the bond lengths Sn(1)–Cl(3) and Sn(2)–Cl(2) reflects the shortening of axial Sn–Cl bonds in a trigonal–bipyramidal ligand polyhedron, with increasing deviation from the ideal geometry towards a monocapped tetrahedron.

Both the Sn–C bond lengths and the bond lengths and angles at the phosphorus atoms show no particularities and agree with values in literature.

The torsion angles in Table 1 indicate that the six-membered chelate rings in **1** adopt a boat conformation. The Rh, P(1), Sn(2) and C(2) atoms are nearly co-planar, and the ring is puckered at the C(1) and Cl(1) edge.

2.3. Structure of *1* in solution

The results of ^{1}H-, ^{31}P- and ^{119}Sn-NMR spectroscopic studies of **1** in C_6D_6 are summarized in Table 2. In solution **1** is monomeric. This is proved by osmometry in C_6H_6 at 45°C (MW measured: 966.5 (Calc. 961.4)) and spectroscopic data. The NMR spectra reveal only one ^{31}P and ^{119}Sn signal and in the ^{1}H-NMR spectrum only one signal is shown for the methyl group protons at the tin atoms. That means, in solution neither an intermolecular Sn(1)···Cl(2′) nor an intramolecular Sn(2)···Cl(1) interaction exists. On the other hand, the high-field shift of the ^{119}Sn-NMR signal (112.6 ppm) and the increase of the $^2J(^1HC^{119}Sn)$ coupling constant (60.2 Hz) compared with the ligand $Me_2(Cl)SnCH_2CH_2PPh_2$ ($\delta_{119Sn} = 142$ ppm, $^2J(^1HC^{119}Sn = 57.8$ Hz [3]) indicate for the tin atoms in **1** at least weak hypervalent contacts. Obviously, **1** undergoes a dynamic process in solution by a fast intramolecular exchange between Rh–Cl(1)···Sn(1) and Rh–Cl(1)···Sn(2) interactions. From the unchanged ^{1}H-NMR spectrum follows that even at −70°C this process is fast within the NMR time scale.

As a consequence of the natural abundance of the ^{119}Sn isotope of 8.58% the dominant isotopomer of **1** in solution contains only one ^{119}Sn atom (the portion of the isotopomer with two ^{119}Sn atoms is 0.74%). That means the ^{119}Sn-NMR spectrum and the satellite part of the ^{31}P-NMR spectrum of **1** are parts of an AA′X spin system (A,A′ = ^{31}P, X = ^{119}Sn) because the two phosphorus atoms are chemically but not magnetically equivalent. Computer simulation gave the coupling constants $^2J(^{31}P, ^{31}P) = 338.9$ and $^3J(^{31}P, ^{119}Sn) = 203.2$ Hz.

2.4. Intramolecular oxidative addition reaction of *1*

Heating **1** in toluene for 2 days at 100°C the formerly yellow solution turns to orange and after evaporation to dryness the yellow rhodium(III) complex [{Me(Cl)Sn$\overline{CH_2CH_2PPh_2}$}$_2$Rh(CO)Cl] (**2**) could be isolated (Eq. (2)). Recrystallization from CH_2Cl_2/hexane yields a pure product.

$$\underset{\mathbf{1}}{[\{Me_2(Cl)SnCH_2CH_2PPh_2\}_2Rh(CO)Cl]} \xrightarrow[-CH_4,\ -C_2H_4]{\text{toluene/100°C/2d}} \underset{\mathbf{2}}{[\{Me(Cl)Sn\overline{CH_2CH_2PPh_2}\}_2Rh(CO)Cl]} \quad (2)$$

The yellow crystals melt at 155°C and are soluble in aromatic and chlorinated hydrocarbons. A strong absorption at 2047 cm^{-1} in the CO valence

Table 2
Characteristic NMR data for **1** and **2**

Compound	Solvent	$\delta(^{119}Sn)$ (ppm)	^{n}J(Sn, Rh) (Hz)	^{n}J(Sn, P) (Hz)	$\delta(^{31}P)$ (ppm)	^{2}J(PRhP) (Hz)	^{1}J(PRh) (Hz)	^{n}J(P, Sn) (Hz)	$\delta(^{1}H)(SnCH_3)$ (ppm)	^{2}J(HCSn) (Hz)
1	C_6D_6	112.6(m)	<1 [a,b]	203.2 [a,c]	30.5(d)	338.9 [a]	122.1	198.7 [a,c]	0.56(s)	60.2
2	CD_2Cl_2	319.4('t') (Sn1) [e]	331.9 [d]	84.3/96.6 [a]	54.8(m)	310.5	92.5	84.6/93.3 [a]	−0.28(s)	56.8
		249.7(m) (Sn2) [e]	221.9 [d]	118.4/145.1 [a]	63.9(m)		90.1	113.7/141.3 [a]	0.05(s)	56.5

[a] Calculated.
[b] ^{4}J(SnCCPRh).
[c] ^{3}J(SnCCP).
[d] ^{1}J(SnRh).
[e] Atom-numbering, see Fig. 2.

region of the IR spectrum of **2** in CsBr indicates the change of **1** to a rhodium(III) complex [2,18].

2.5. Molecular structure of [{Me(Cl)SnCH$_2$CH$_2$PPh$_2$}$_2$Rh(CO)Cl] (2)

The solid state structure of **2** consists of discrete monomeric units separated by normal van der Waals contacts. An overall view of the molecule with the atom-numbering scheme is shown in Fig. 2. Selected bond lengths and angles are listed in Table 3. The main feature of the structure of **2** are the two five-membered P, Sn, and Rh containing heterocycles with a covalent tin–rhodium bond and the short Sn(2)···Cl(1) contact of 3.140(3) Å (sum of the van der Waals radii: 3.85 Å [15]). The rhodium atom is situated in an octahedral ligand sphere. The two phosphorus atoms are *trans* and the tin atoms are *cis* to one another. The octahedron is distorted at the Cl(1) edge by the Cl(1)···Sn(2) interaction (Cl(1)–Rh–Sn(2) 75.1(1)°, Cl(1)–Rh–C(5) 105.4(1)°, Cl(1)–Rh–Sn(1) 160.7°(1)) and by the P–Rh–Sn angle depression as result of the chelate ring formation (P(1)–Rh–Sn(1) 83.6(1)°, P(2)–Rh–Sn(2) 83.5(1)°). The Sn–Rh bond lengths agree with values described in the literature [16,17]. Due to the higher *trans* influence of the CO ligand compared with that of the Cl ligand the Rh–Sn(2) distance is with 2.634(1) Å sligthly longer than the Rh–Sn(1) bond length (2.592(1) Å). Both the two phosphorus and the two tin atoms exhibit a tetrahedral coordination, but, the deviation from the ideal geometry is in case of the tin atoms higher.

The five-membered chelate rings show an envelope conformation. Sn, P, Rh and one C atom nearly form a plane, and one ring is puckered at the C(1) and the other one at the C(4) atom.

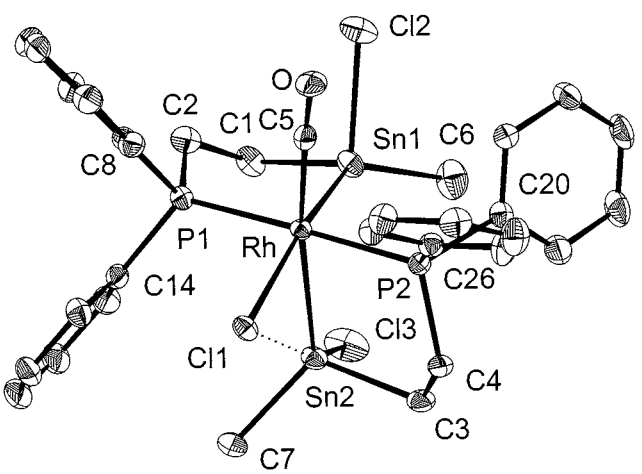

Fig. 2. Molecular structure of [{MeSnCH$_2$CH$_2$PPh$_2$}$_2$Rh(CO)Cl] (**2**) with the atom-labeling scheme. Hydrogen atoms and the solvent molecule (C_6H_6) are omitted for clarity.

Table 3
Selected bond lengths (Å), angles (°) and endocyclic torsion angles (°) for [{MeSnCH$_2$CH$_2$PPh$_2$}$_2$Rh(CO)Cl] (**2**)

Bond lengths (Å)			
Rh–Sn(1)	2.592(1)	Sn(2)–C(3)	2.168(5)
Rh–Sn(2)	2.634(1)	Sn(2)–C(7)	2.135(5)
Rh–P(1)	2.370(1)	Sn(2)–Cl(3)	2.474(1)
Rh–P(2)	2.365(1)	P(1)–C(2)	1.856(5)
Rh–C(5)	1.942(4)	P(1)–C(8)	1.840(4)
Rh–Cl(1)	2.514(1)	P(1)–C(14)	1.837(4)
Sn(1)–C(1)	2.159(5)	P(2)–C(4)	1.842(4)
Sn(1)–C(6)	2.133(7)	P(2)–C(20)	1.835(5)
Sn(1)–Cl(2)	2.430(1)	P(2)–C(26)	1.836(4)
Bond angles (°)			
P(1)–Rh–P(2)	178.8(1)	C(6)–Sn(1)–Cl(2)	100.8(2)
Sn(1)–Rh–Cl(1)	160.7(1)	Rh–Sn(2)–C(3)	102.1(1)
Sn(2)–Rh–C(5)	172.2(1)	Rh–Sn(2)–C(7)	128.0(2)
Sn(1)–Rh–Sn(2)	86.5(1)	Rh–Sn(2)–Cl(3)	115.4(1)
Sn(1)–Rh–P(1)	83.6(1)	C(3)–Sn(2)–C(7)	113.0(2)
Sn(1)–Rh–P(2)	96.5(1)	Cl(3)–Sn(2)–Cl(3)	98.4(1)
Sn(1)–Rh–C(5)	93.6(1)	C(7)–Sn(2)–Cl(3)	96.5(2)
Sn(2)–Rh–P(1)	95.3(1)	Rh–P(1)–C(2)	114.2(2)
Sn(2)–Rh–P(2)	83.5(1)	Rh–P(1)–C(8)	113.5(1)
Sn(2)–Rh–Cl(1)	75.1(1)	Rh–P(1)–C(14)	117.2(1)
P(1)–Rh–C(5)	92.4(1)	C(2)–P(1)–C(8)	102.6(2)
P(1)–Rh–Cl(1)	92.1(1)	C(2)–P(1)–C(14)	105.2(2)
P(2)–Rh–C(5)	88.7(1)	C(8)–P(1)–C(14)	102.6(2)
P(2)–Rh–Cl(1)	87.4(1)	Rh-P(2)-C(4)	113.5(2)
C(5)-Rh-Cl(1)	105.4(1)	Rh-P(2)–C(20)	116.4(1)
Rh–Sn(1)–C(1)	101.1(1)	Rh–P(2)–C(26)	114.6(1)
Rh–Sn(1)–C(6)	131.1(2)	C(4)–P(2)–C(20)	106.1(2)
Rh–Sn(1)–Cl(2)	105.8(1)	C(4)–P(2)–C(26)	102.9(2)
C(1)–Sn(1)–C(6)	114.4(2)	C(20)–P(2)–C(26)	101.7(2)
C(1)–Sn(1)–Cl(2)	99.1(1)		
Torsion angles (°)			
Rh–P(1)–C(2)–C(1)	36.6(4)	Rh–P(2)–C(4)–C(3)	44.8(4)
P(1)–C(2)–C(1)–Sn(1)	−50.1(4)	P(2)–C(4)–C(3)–Sn(2)	−41.9(4)
C(2)–C(1)–Sn(1)–Rh	41.6(3)	C(4)–C(3)–Sn(2)–Rh	22.3(3)
C(1)–Sn(1)–Rh–P(1)	−16.5(1)	C(3)–Sn(2)–Rh–P(2)	1.4(1)
Sn(1)–Rh–P(1)–C(2)	−4.9(2)	Sn(2)–Rh–P(2)–C(4)	−21.2(2)

2.6. NMR spectroscopy of 2

The NMR data in Table 2 indicate that the structure of **2** in solution is identical with that in the solid state. Furthermore, the molecular geometry causes the chemical nonequivalence both of the two tin and phosphorus atoms and also of the two tin methyl groups and the eight methylene protons in the chelate rings. Because of the proportion of only 8.58% for the NMR active ^{119}Sn isotope (see Section 2.3) three isotopomers of **2** with the spin systems ABX, ABLX, and ABMX (A, B = ^{31}P, L = ^{119}Sn(1), M = ^{119}Sn(2), X = ^{103}Rh) exist. Therefore, the main signals in the ^{31}P-NMR spectrum which are doubled by the P–Rh coupling represent the AB part of the ABX spin system (δ: 54.8 ppm, $^1J(^{31}P^{103}Rh)$ = 92.5 Hz; δ: 63.9 ppm, $^1J(^{31}P^{103}Rh)$ = 90.1 Hz). The decrease of the $^1J(^{31}P^{103}Rh)$ coupling constant for **2** compared with **1** demonstrates the increase in the oxi-

dation state from Rh(I) to Rh(III) [18]. The ^{119}Sn satellite signals in the ^{31}P-NMR spectrum represent the AB part of the ABLX and the ABMX spin systems mentioned above. At the present stage of our studies an assignment of the ^{31}P-NMR signals is not possible.

The ^{119}Sn-NMR spectrum exhibits a multiplet at 249.7 ppm and a virtual triplet at 319.4 ppm. Both signals are doubled by Sn–Rh coupling. The assignment of the two ^{119}Sn-NMR signals is based on the different *trans* influence of the CO and the Cl ligand. With respect to the higher *trans* influence of CO (see Section 2.2) the $^{1}J(^{119}\mathrm{Sn}(2)^{103}\mathrm{Rh})$ coupling constant of 221.9 Hz is 110 Hz smaller than the $^{1}J(^{119}\mathrm{Sn}(1)^{103}\mathrm{Rh})$ coupling. Therefore, the high-field ^{119}Sn-NMR signal at 249.7 ppm can be assigned to the Sn(2) atom and the signal at 319.4 ppm to the Sn(1) atom. The low-field position of the latter signal is also in agreement with the high electronegativity of the Cl atom in the *trans* position. Each ^{119}Sn nucleus couples with both phosphorus nuclei, but, in a different way. The $^{2}J(^{119}\mathrm{SnRh}^{31}\mathrm{P})$ is the one coupling the other one $^{n}J(^{119}\mathrm{Sn},\ ^{31}\mathrm{P})$ represents the sum of the two contributions $|^{2}J(^{119}\mathrm{SnRh}^{31}\mathrm{P})|$ and $|^{3}J(^{119}\mathrm{SnCC}^{31}\mathrm{P})|$ within the chelate ring. The coupling constants are determined by computer simulation using the ^{119}Sn-NMR spectrum and the satellite part of the ^{31}P-NMR spectrum. As mentioned above an assignment of the $^{n}J(^{119}\mathrm{Sn},\ ^{31}\mathrm{P})$ coupling constants to a certain phosphorus atom is not possible.

The significant down field shift both of the ^{31}P and the ^{119}Sn-NMR signals is due to the fact that these atoms are included in a five-membered ring ('ring effect' of chemical shifts [19]). We have observed the same effect for the bicyclic platinum complex $[\{Me_2\overline{SnCH_2CH_2PPh_2}\}_2Pt]$ [4].

The values of 211 and 224 Hz, respectively, for the ^{n}J(H, Sn) coupling constant for two of the four PCH_2-protons in the chelate rings of **2** are remarkably high.

Our knowledge about the mechanism of the transformation of **1** into **2** is only vague. Certainly, the first step is the intramolecular oxidative addition of the Sn–C(Me) bond of one ligand to the Rh(I) centre of **1**. Efforts to detect the resulting intermediate complex failed. The higher reactivity of a Sn–C bond compared with a Sn–Cl bond in oxidative additions of triorganotin halides also is described for the reaction of R_3SnCl with Pd^0 and Pt^0 complexes [20]. The intramolecular rearrangement of the intermediate complex to **2** by demethylation both of the Rh atom and the tin atom of the second ligand is accompanied by the formation of methane and ethylene in a molar ratio of 2:1. This could be proved by gas-chromatographic investigation of the reaction.

3. Experimental

All manipulations were performed under dry argon. Elemental analyses were carried out at the Microanalytical Laboratory of the Chemical Department. Infrared spectra were measured on a Specord 75 IR (CsBr). The NMR spectra were recorded on Gemini 200 (Varian) or Unity 500 (Varian) spectrometers. Solvent signals (^{1}H, ^{13}C), Me_4Sn (^{119}Sn) and 85% H_3PO_4 (^{31}P) were used as references. The NMR spectra simulations were performed with the program PERCH [21]. The molecular weight determination of **1** was performed in benzene at 45°C (concentration = 0.01 mol l^{-1}) using a Knauer osmometer.

3.1. $[\{Me_2(Cl)SnCH_2CH_2PPh_2\}_2Rh(CO)Cl]$ (1)

Solutions of $[Rh(CO)_2Cl]_2$ (300 mg, 0.77 mmol) and $Me_2(Cl)SnCH_2CH_2PPh_2$ [3] (613 mg, 1.54 mmol) in benzene (in each case 10 ml) are dropped simultaneously in pure benzene (50 ml) and the mixture is stirred for 2 h to give a light yellow solution. During the reaction the equivalent amount of CO (35 ml) is released. After evaporation of the solvent the residue is washed with pentane and dried in vacuo. **1** is obtained as a yellow fine-crystalline compound (1.4 g, 96%); m.p. 124–126°C.

$C_{33}H_{40}Cl_3OP_2RhSn_2$ (961.3): anal. (exp./calc.) C, 41.51/41.23; H, 4.22/4.19; IR (CsBr, cm^{-1}): 1975 (CO). ^{1}H-NMR (C_6H_6): δ 0.56 (s, 6H, $SnCH_3$, ^{2}J(H, Sn) 60.2 Hz); 1.43 (m, 4H, $SnCH_2$); 2.84 (m, 4H, PCH_2, ^{3}J(H, Sn) 70 Hz); 6.99–7.68 (m, 20H, PC_6H_5) ppm.

3.2. $[\{Me(Cl)\overline{SnCH_2CH_2PPh_2}\}_2\overline{Rh(CO)Cl}]$ (2)

A solution of **1** (1.0 g, 1.04 mmol) in toluene (50 ml) was heated under stirring for 2 days whereby it slowly turned from yellow to orange. The solvent was removed and the yellow residue recrystallized from CH_2Cl_2/hexane giving pure **2** (560 mg, 61%); m.p. 155°C.

$C_{31}H_{34}Cl_3OP_2RhSn_2$ (931.2): anal. (exp./calc.) C, 40.53/39.98; H 4.53 /3.68; Cl 11.42/12.03; IR (CsBr, cm^{-1}): 2047 (CO). ^{1}H-NMR (CD_2Cl_2): δ −0.28 (s, 3H, $SnCH_3$, ^{2}J(H, Sn) 56.8 Hz); 0.05 (s, 3H, $SnCH_3$, ^{2}J(H, Sn) 56.5 Hz); 1.46 (m, 1H, $SnCH_2$); 1.84 (m, 2H, $SnCH_2$); 1.92 (m, 1H, $SnCH_2$); 2.35 (m, 1H, PCH_2); 2,58 (m, 1H, PCH_2); 2.96 (m, 1H, PCH_2, ^{3}J(H, Sn) 211 Hz); 3.60 (m, 1H, PCH_2, ^{3}J(H, Sn) 224 Hz); 7.37–8.20 (m, 20H, PC_6H_5) ppm.

3.3. Crystallographic studies

Crystal data and details of the data collection and refinement of **1** and **2** are summarized in Table 4.

Table 4
Crystal data and details of data collection and refinement for **1** and **2**

	1	**2**
Formula	$C_{33}H_{40}Cl_3OP_2RhSn_2$	$C_{34}H_{37}OCl_3RhSn_2$
Formula weight (g mol^{-1})	961.23	970.22
Space group	$P2_1/c$	$P2_1/n$
Temperature	240 K	r.t.
Lattice parameters		
a (Å)	18.590(10)	13.521(2)
b (Å)	11.514(3)	10.499(1)
c (Å)	18.812(8)	25.761(2)
β (°)	107.66(5)	91.574(13)
Cell volume (Å^3)	3837(3)	3655.4(8)
Formula units/unit cell	4	4
$D_{calc.}$ (g cm^{-1})	1.664	1.763
2θ Range (°)	4.22–52.30	4.18–51.74
Range of h, k, l	−23 to 23; −12 to 14; −22 to23	−16 to 16; −12 to 12; −31 to 31
Reflections measured	24131	26217
Reflections unique	7488	6804
Reflections observed ($I_o \geq 2.0\sigma(I_o)$)	5147	
R_{int}	0.0611	0.0717
Data/parameters	7488/522	6804/520
Goodness-of-fit (F^2)	0.922	1.075
R_1/wR_2 (F^2) (all data)	0.0615/0.0691	0.0396/0.0923
R_1/wR_2 (F^2) ($I_o \geq 2.0\sigma(I_o)$)	0.0329/0.0621	0.0302/0.0746
Min./max. residual electron density (e Å^{-3})	−0.388/0.745	−0.754/1.327

Intensities were collected on a STOE IPDS diffractometer using Mo–K_α radiation ($\lambda = 0.71073$ Å). Final lattice parameter were obtained from a least square refinement using 5000 reflections. The structures were solved by direct methods using the program SHELXS-86 [22]. The full-matrix least square structure refinement was performed with the program SHELXL-93 [23]. All non-H atoms were refined anisotropically. Figures were drawn with the program DIAMOND 2.0 [24].

Acknowledgements

The authors thank the Deutsche Forschungsgemeinschaft and the Fonds der Chemischen Industrie for financial support.

References

[1] H. Weichmann, G. Quell, A. Tzschach, Z. Anorg. Allg. Chem. 462 (1980) 7.
[2] J. Grobe, R. Martin, G. Huttner, L. Zsolnai, Z. Anorg. Allg. Chem. 607 (1992) 146.
[3] H. Weichmann, J. Organomet. Chem. 262 (1984) 279.
[4] H. Weichmann, J. Organomet. Chem. 238 (1982) C49.
[5] C. Müller, U. Schubert, Chem. Ber. 124 (1991) 2181.
[6] U. Schubert, S. Grubert, U. Schulz, S. Mock, Organometallics 11 (1992) 3163.
[7] U. Schubert, S. Grubert, Organometallics 15 (1996) 4707.
[8] U. Baumeister, H. Hartung, T. Schulz, H. Weichmann, Acta Cryst. C54 (1998) 333.
[9] J. Grobe, E.M. Reifer, B. Krebs, M. Läge, Z. Anorg. Allg. Chem. 623 (1997) 264.
[10] T. Schulz, H. Weichmann, U. Baumeister, A. Krug, H. Hartung, J. Organomet. Chem. (in preparation).
[11] A.A.H. Van der Zeijden, G. Van Koten, J.M.A. Wouters, W.F.A. Wijsmuller, D.M. Grove, W.J.J. Smeets, A.L. Spek, J. Am. Chem. Soc. 110 (1988) 5354.
[12] F. Dahan, R. Choukroun, Acta Cryst. C41 (1985) 704.
[13] M. Dräger, J. Organomet. Chem. 251 (1983) 209.
[14] U. Kolb, M. Dräger, B. Jousseaume, Organometallics 10 (1991) 2737.
[15] A. Bondi, J. Phys. Chem. 68 (1964) 441.
[16] H. Werner, O. Gevert, P. Haquette, Organometallics 16 (1997) 803.
[17] L. Carlton, R. Weber, D.C. Levendis, Inorg. Chem. 37 (1998) 1264.
[18] D.L. Egglestone, M.C. Baird, C.J.L. Lock, G. Turner, J. Chem. Soc., Dalton Trans. (1977) 1576.
[19] P.E. Garrou, Chem. Rev. 81 (1981) 229.
[20] C. Eaborn, A. Pidcock, B.R. Steele, J. Chem. Soc., Dalton Trans. (1976) 767.
[21] PERCH, NMR Software, Version 3/98, © University of Kuopio, Finland.
[22] G.M. Sheldrick, SHELXS-86, Program for the solution of crystal structures, University of Göttingen, Germany (1986).
[23] G.M. Sheldrick, SHELXL-93, Program for the refinement of crystal structures, University of Göttingen, Germany (1993).
[24] K. Brandenburg, DIAMOND 2.0,Visual crystal structure information system, crystal impact, Bonn, Germany (1998).